Two-way multi-band optical/IR transmission measurements in the Persian Gulf-Coastal Region

Arie N. de Jong, Peter J. Fritz

TNO-Defence, Security and Safety, The Hague – Netherlands

ABSTRACT

The atmospheric conditions in the Persian Gulf region are significantly different from other places in the world. The particle size distribution may vary daily and during the day. The aerosols can contribute to the amount of rainfall over land, important for the nations around the Gulf. In 2004 NASA/GSFC and NRL (Naval Research Laboratory) introduced a proposal to improve the modelling of aerosol transport for the Persian Gulf area. The proposal included a measurement campaign in the UAE (United Arabian Emirates), held in the summer/fall of 2004, sponsored by the DWRS (Department of Water Resources Studies) in Abu Dhabi: UAE² (Unified Aerosol Experiment in the UAE). In this campaign NASA installed a number of multi-spectral sun-photometers at various locations in the UAE (**http://aeronet.gsfc.nasa.gov**). NRL installed ground based and airborne particle samplers. In addition, TNO (the Netherlands) installed its multi-band optical/IR transmissometer, in order to collect horizontal, path-integrated transmission data. This device provides additional information on the scattering behaviour of the aerosols compared to the other instruments, which either integrate scattering over the full vertical path (the NASA sun-photometers, providing the Aerosol Optical Depth (AOD)) or sample the particles in-situ (the NRL particle samplers, providing size distribution and composition).

This paper deals with our transmission measurement set-up, which was located in a coastal area near Abu Dhabi. This location allowed the investigation of the local variability of the atmospheric conditions: from desert dust to pollution, such as fossil fuel and biomass burning, depending on the wind direction. For logistic reasons a set-up was chosen with a retro-reflector. This choice implies consequences for the calibration procedure and measurement accuracy, which are discussed in detail. Also the effects of path-inhomogeneity and scintillation for such a two-way set-up are considered. Results are presented for the measurement period of two weeks in September, showing interesting transmission effects due to temporal changes in aerosol particle composition. These phenomena cannot be explained by scattering theory for spherical particles. More knowledge is required on the shape and composition of the particles. Comparison of the transmission data with the data from other instruments will be done in a next phase.

Keywords: atmospheric transmission, aerosols, dust, sea salt, pollution, transmission measurement, retro-reflector

1. INTRODUCTION

Very few data are available on the low-level optical and infrared transmission characteristics of the atmosphere in the Persian Gulf area. When users want to predict the optical/IR transmission in a certain spectral band, they tend to use models such as Modtran, while introducing parameters such as air temperature, humidity, visibility and type of aerosol (air mass parameter). This model is well validated for geographical locations on earth such as the North Atlantic Ocean, the Caribbean and the Mediterranean Sea. For areas such as the Persian Gulf however, large uncertainties exist about the nature of the aerosol particles. Contributions arrive from the desert (dust particles) and the (oil) industry, producing smoke plumes with more or less hygroscopic particles with various compositions (e.g. sulphates and soot). It is not certain, what the effect of the high water temperature (up to 34 °C) is on their particle size distribution. Most of these particles have a non-spherical shape and an unknown (complex) refractive index [1], which excludes the proper use of standard Mie-scattering and extinction calculations. An additional problem is the rapid daily and hourly changes in atmospheric conditions (visibility) due to the land-sea breeze effects. Influences of large-scale weather systems such as high-pressure systems from Siberia and the Indian Ocean, troughs from the Red Sea and the Mediterranean Sea and a thermal low-pressure area, present above the Persian Gulf cause a large variability in weather conditions in the area. On a regional scale these systems tend to produce an atmospheric condition with large concentrations of aerosols of various nature: dust and smoke particles from the oil industry, possibly acting as condensation nuclei, being a source of rain.

The DWRS of the United Arabian Emirates (UAE) contacted therefore the University of Witwatersrand in South Africa to study the local atmospheric conditions in general and the possibilities of cloud seeding (rain making) in particular. On the AERONET website (Holben, NASA) retrieval algorithms, applied to the sun-photometer data for this area (only day-time!), show predicted particle size distributions with frequent presence of particles with a size of 3 μm and more. Particles with this size have a big impact on the transmission in the infrared part of the spectrum. The AERONET data are retrieved for a vertical optical path through the total atmosphere, so they are not directly applicable to the particle size distributions at low-level horizontal paths. It is also noted that the AERONET sensors are only working in the visible and near IR part of the spectrum. Nevertheless we found it very interesting for TNO to participate in the UAE[2] trials, organised by NASA/GSFC with contributions from NRL and NCAR (National Centre for Atmospheric Research) and sponsored by DWRS. Our transmission data may provide additional information on the optical characteristics of the particles in the measurement path and support the propagation modelling. Aerosol extinction is one of the essential elements in the prediction of the range performance of optical and infrared sensors.

The benefit of using a multi-band transmissometer system has been demonstrated before in the VAMPIRA trials [2]. Wavelength dependent extinction coefficients could be recorded during conditions with changing visibility for an overseas path with mainly aerosols, consisting of spherical water particles. It is well known that extinction by scattering is dependent on the size of the particles compared to the wavelength considered [3]. The seven spectral bands of the TNO transmissometer, ranging from 0.4 to 14 μm, provide a good match with the wide spectral range, corresponding to the expected particle size distributions in the Gulf area. Several technical problems were faced, when planning the set-up of the transmissometer in the Gulf area: the high air temperatures outside in daytime and dust, to which the optical sensors are continuously exposed. Due to the requirement of co-location with the NRL particle measurement station near the harbour of Port Al Sadr, the maximum available range for the transmissometer was 890 m. The location of the set-up in this area is shown on the map in Figure 1. This harbour is located about 50 km Northeast of Abu Dhabi and about 5 km Southwest of the power station of Taweela. On the inland side Port Al Sadr is bordered directly by desert- type landscape, while on the sea side the warm water of the shallow Persian Gulf provides high humidity conditions. The industry of Abu Dhabi and the power station of Taweela tend to provide polluted air masses. The location thus guarantees a great variability in atmospheric composition depending on the wind direction.
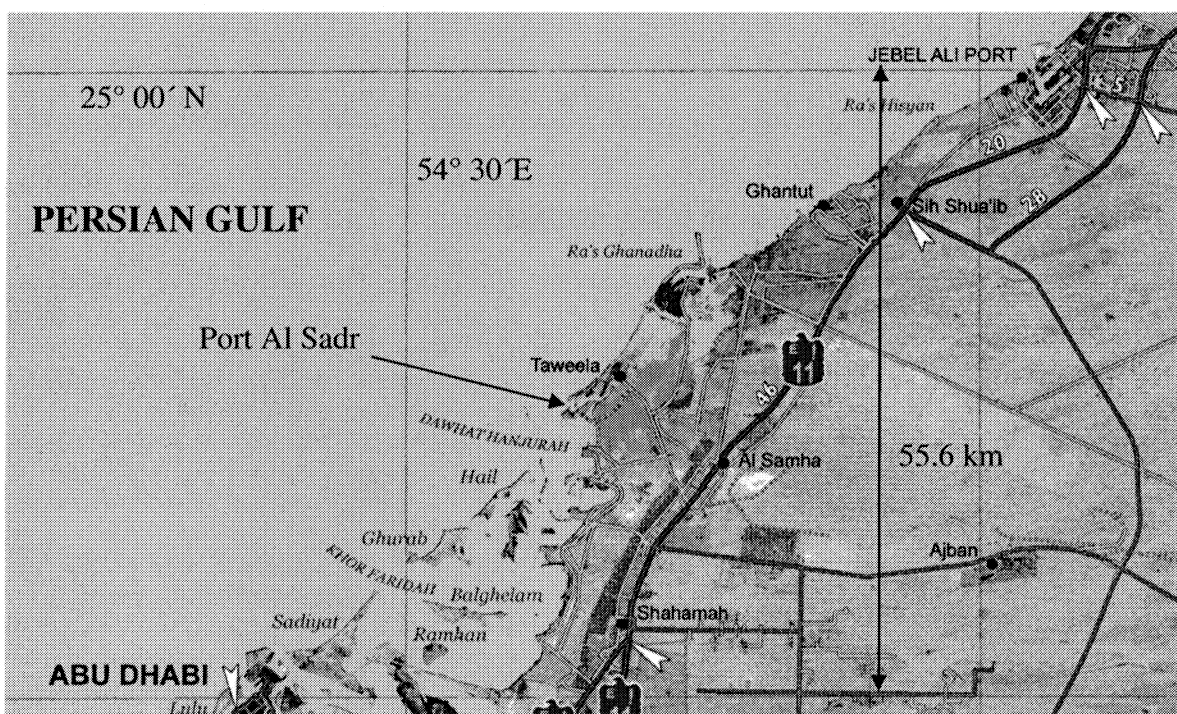

Figure 1. Location of the multi-band optical/IR transmissometer during the UAE[2] trials near Taweela

Because of the short available range, we decided to set-up the system with the source and receiver at the same location and to use a self-supporting retro-reflector at the other end of the path, requiring no external electric power. Technical details on a one-way set-up and this set-up and on the methods of calibration are presented and discussed in sections 2, 3 and 4. In section 5 the implication of the two-way set-up for the effects of scintillation and along path-inhomogeneity on the interpretation of the measurement results and on the accuracy of the data is discussed. Typical samples of the results are shown in section 6, including the variations in the multi-band transmission data due to changing conditions. Section 7 contains a more detailed analysis, including separation of the effect of molecular extinction in order to study more closely the extinction by aerosols and preliminary conclusions.

2. ONE-WAY TRANSMISSOMETRY

The measurement of atmospheric transmission along a single path is rather straightforward when adequate precautions are taken into account during the preparation and calibration procedure [4]. In Figure 2 the principle of a one-way transmissometer is illustrated. A radiating source, positioned near the focal plane of a collimating optical system, having a beam divergence $\delta_s = D_s/f_c$, according to the size of the source D_s and the focal length of the collimator f_c, creates a certain radiation distribution near the receiver, located at a distance R. When the receiver optics is properly aligned in the area of the beam with the maximum irradiance level I_m (in Watt/m²), the power received by the detector, located in the focal plane of an optical unit with diameter D_r and transmission τ_r, is given by $W_d = I_m \times \tau_r \pi D_r^2/4$ (Watt). The irradiance level is determined by the radiant intensity W_i of the source and the transmission of the atmosphere τ_a along the path in a given spectral band: $I_m = W_i \times \tau_a/R^2$; the distance R between source and receiver is large compared to f_c, (eg 1000x). The radiant intensity W_i is determined by the radiance of the source W_s (Watt/m²sr), the diameter D_0 of the optics and the transmission τ_s: $W_i = W_s \times \tau_s \pi D_0^2 /4$ (Watt/sr). The values of Ws, Wi and Wd are all considered as peak radiations in a given spectral band, determined by the spectral emission of the source, the spectral response of the detector and the spectral transmission of the filter.
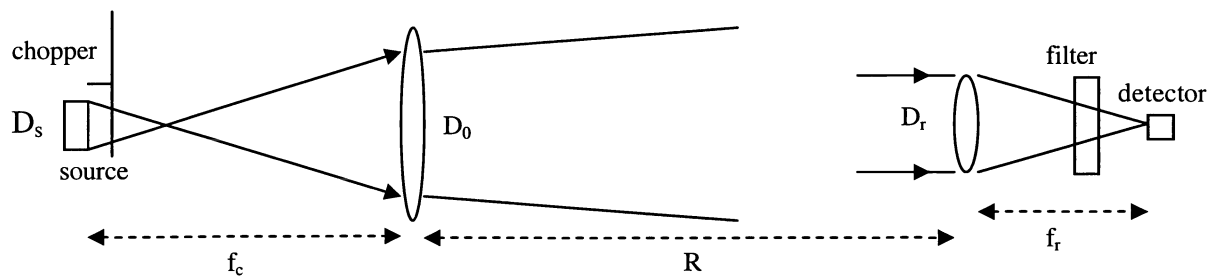

Figure 2. Illustration of single-path set-up for the measurement of atmospheric transmission

It is noted however that the source radiation is modulated by means of a chopper, resulting in a trapezium form of signal, implying a certain so-called chop-factor, converting the peak signal into a rectified and time-averaged signal. A pick-up takes care of a reference signal, transmitted to the receiver side by radio. The detector pre-amplifier may transform the signal somewhat because of its limitation of the electronic bandwidth. A demodulator, consisting of a bi-directionally rectifying and averaging circuit, creates a DC output signal V_d (in Volts), which is proportional to I_m: $V_d = \rho I_m$, where ρ is the responsivity (V/Watt/m²), which includes the chop-factor. Generally the sensitivity of the receiver is given as its Noise Equivalent Irradiance NEI (Watt/m²), defined by the ratio of the RMS noise level N after the demodulator and the responsivity. The NEI can be expressed in terms of the optical and electronic parameters of the receiver by the formula: NEI = $(D_d\sqrt{2}) / (\pi \tau_r D_r^2 D^*\sqrt{\tau_i})$, where D_d is diameter of the detector, related to the field of view Φ (in radian) and the focal length of the optics f_r by $D_d = \Phi \times f_r$. In the formula for NEI, D* is the detectivity of the detector in mHz$^{1/2}$Watt^{-1} and τ_i is the integration time, applied in the averaging circuit. With the expressions, given so far, it is possible to specify the signal to noise ratio V_d/N of the transmissometer as function of the source radiant intensity W_i, the atmospheric transmission τ_a, the range R and the sensitivity NEI:

$$V_d/N = \rho I_m / \rho NEI = W_i \times \tau_a / (R^2 \times NEI) \qquad (1)$$

This formula allows the design of the set-up of the system at any location. The values of W_i and NEI, together with some of the other basic parameters of the Multi-Spectral Radiometer Transmissometer (MSRT) system, are listed in Table 1. The parameters of the receiver optics deviate from those, given in [2]. Also the value of W_i is different due to a change in radiating elements. The chop-factor is such, that a 1 Volt trapezium type of peak signal after the pre-amplifier gives a DC averaged output signal of 2.5 Volt, while a square wave signal gives 3.6 Volt. The integration time τ_i of the signal averaging unit, in which N and NEI are determined, has been set to 1.1 second. If, for example, we want to measure the atmospheric transmission in channel 7 with an accuracy of 1%, the range at which this occurs appears to be 8.1 km. All other channels provide data with higher accuracy at this range.

Table 1. Basic characteristics of the MSRT multi-band transmissometer, used in the UAE[2] measurement campaign

Channel	Spectr. band (FWHM)	W_i (peak)	Receiver Optics			Resp. ρ	Noise N	NEI
No	μm	Watt/sr	f_r mm	Φ mrad	D_r mm	kV/W/m² @G1	μV(RMS) @G1	nW/m²
1	0.40-0.49	250	120	21.2	38	1.21	11.5	9.5
2	0.57-0.65	850	120	22.5	38	6.28	21	3.3
3	0.78-1.04	3350	120	22.5	38	6.53	20	3.1
4	1.39-1.67	2560	120	25.0	38	12.5	42	3.4
5	2.12-2.52	1060	40	25.0	16	0.295	4.6	16
6	3.55-4.15	287	125	16.0	55	13.9	16	1.15
7	7.8-13.7	67	75	26.7	75	0.513	5.3	10.3

3. TWO-WAY TRANSMISSOMETRY

In the case of the use of co-location of source and receiver on one side of the measurement path and a retro-reflector on the other side at a distance R, a set-up is created as schematically shown in Figure 3. As the source and receiver cannot really be co-located without the use of a beam splitter, which we want to avoid, the entrance pupil of the receiver is somewhat dislocated over a distance of a little more than the sum of half of the size of the pupils of the source and the receiver. For the retro-reflector an optical system consisting of mirrors is preferred, including a mirror near the focal plane, allowing the variation of the divergence of the return beam. This divergence should be large enough to cover the dislocated pupil of the receiver. The retro-reflector used here and shown in more detail in Figure 4 is preferred in favour of corner reflectors, as they do not allow the variation of the divergence of the return beam. A disadvantage of the set-up is that the receiver entrance is not located in the centre of the area with the maximum returning irradiance level.
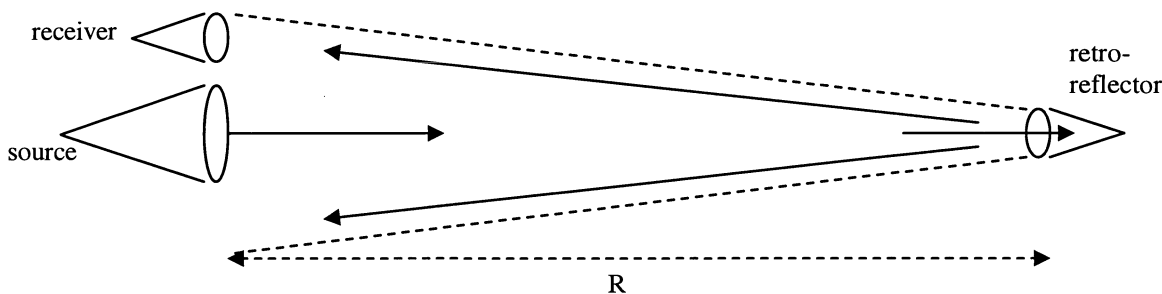

Figure 3. Principle of a bi-static two-way transmissometer set-up with source and receiver on one side and retro-reflector, located on the other side of the measurement path; the total atmospheric path-length becomes 2R.

The retro-reflecting collimator consists of a main parabolic mirror with a diameter D=20 cm and a focal length f =50 cm. A 45° flat folding mirror directs the incoming beam to a small flat mirror M, which is displaced over a small distance d near the focal plane. This displacement leads to a total beam divergence δ of the return beam of δ = D x $2d/f^2$. If the path-length is 1000 m and the distance of the edge of the receiver lens to the centre of the source is 0.5 m, δ should be 1 mrad, so the displacement d becomes 0.625 mm. Due to optical aberrations of the retro-reflector, the real beam divergence of the return beam is larger and leads to a gradual fall-off of the irradiance level outside the centre of the return beam. It is noted that a mechanical shutter is adopted in front of the small mirror M, in order to allow a check if any other retro-reflection occurs, for example backscatter in the case of foggy conditions. The shutter opens and closes the return beam each minute for one minute. An advantage of the mirrors in the retro-reflector is that they work similar over the whole spectral band of the MSRT system.
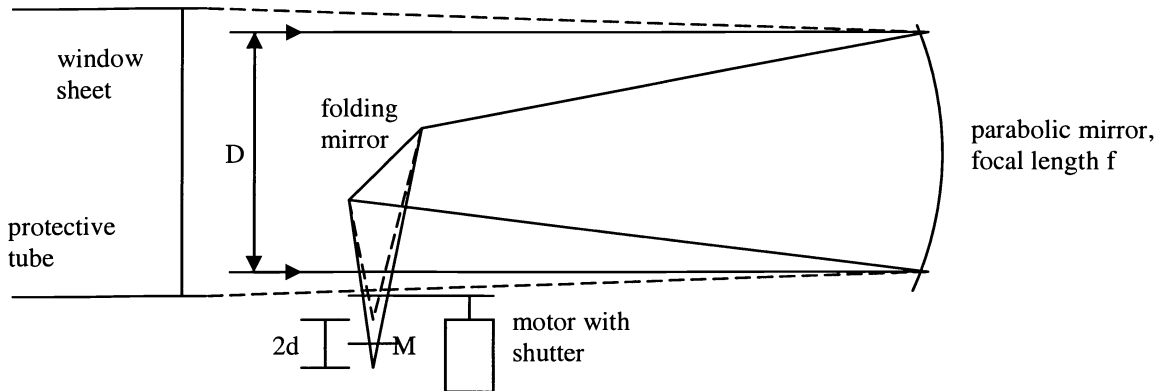

Figure 4. Principle of retro-reflecting collimator with shutter and small mirror M near the focal plane

It is noted that the source in reality consists of two beams, one for the visual and one for the IR channels. In order to obtain a good understanding of the positioning of the two exit and seven entrance pupils, a schematic illustration is given in Figure 5. The irradiance level I at the entrance of the receivers is determined by the diameter of the return beam δR, the diameter of the retro-reflector D, its optical transmission τ and the atmospheric transmission over the path-length 2R.
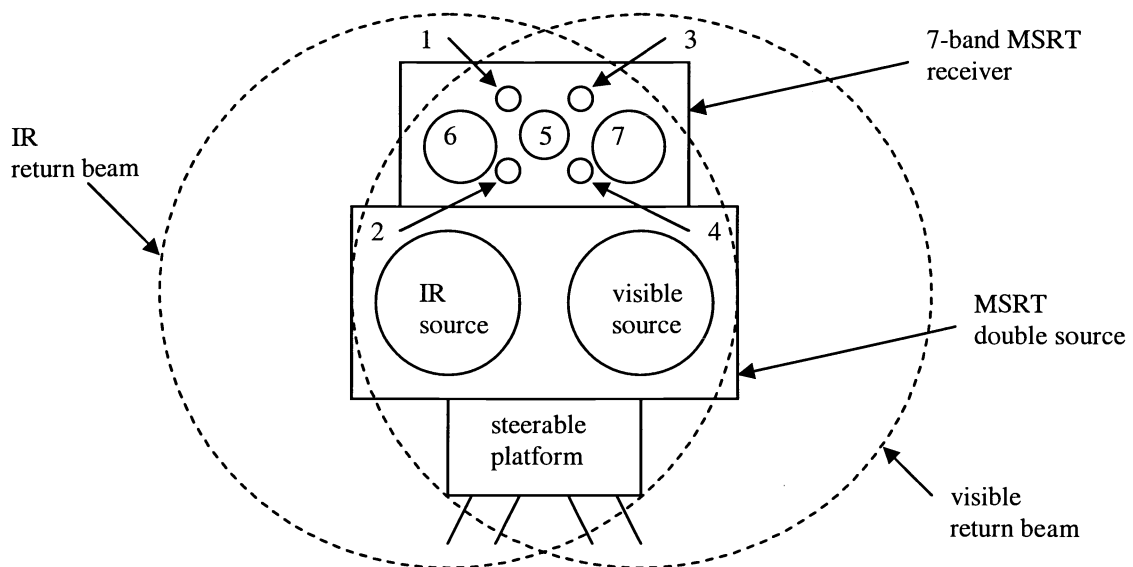

Figure 5. Front view of the pupil and beam positioning; both return beams should cover all seven pupils of the receiver

$$I = W_i \times \tau D^2 \times \tau_a(2R) \; / \; \{R^2 \times (\delta R)^2\} \tag{2}$$

Compared to the irradiance level I_m for a one-way transmissometer set-up over the same path-length 2R, I is a factor $\tau(D/\delta R)^2$ smaller. If we take for example $\tau = 1$, $\delta = 0.001$, $R = 1000$ m and $D = 0.2$ m, the loss ratio I/I_m becomes 0.04 which means a factor 25 loss in irradiance level. In reality τ is considerably less than 1 due to reflection losses at the mirrors and the obscuration of the folding mirror. For the retro-reflector that we used in the UAE² campaign, the average value of τ was 0.4; for channel 1 this was less, as one of the mirrors had a gold coating. It is interesting to note that the loss ratio is independent of the range if the diameter (δR) of the return beams is kept constant. Pictures of the optical equipment, as set-up during the UAE² campaign, are shown in Figure 6. The real distance between the source/receiver and the retro-reflector was 890 m, which was more than 90% over (harbour) water. For δR a value of 0.6 m is estimated.
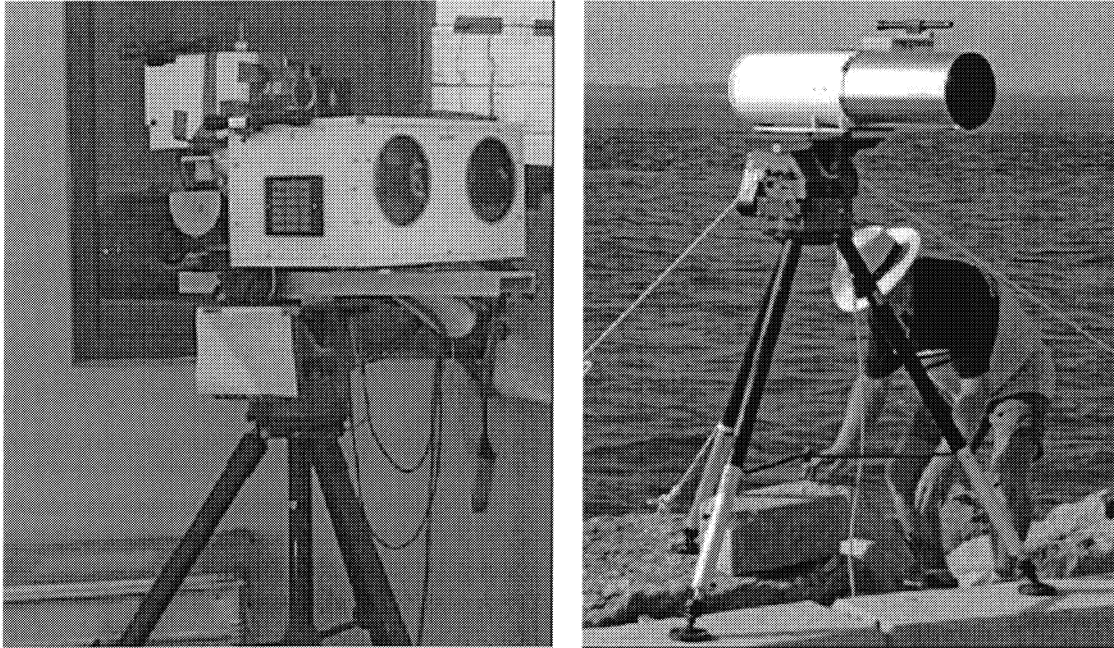

Figure 6. Pictures showing the set-up of the source and receiver (left) and the retro-reflector (right) during the UAE² trial

4. CALIBRATION PROCEDURE

Calibration of a transmissometer system is a non-trivial issue. Even if all optical parameters, such as presented in Sections 2 and 3, are known, systematic errors may occur. In the ideal situation the signal level over the same path should be measured without and with atmospheric attenuation. In some cases, when the pupils of the source and receiver have the same size, both optical systems could be placed face to face at zero range in the laboratory, as was done by Zeisse [5]. In our case the receiver pupils are smaller than the source pupil, so they are unable to collect all the radiation at zero range. When applying laboratory calibration, a couple of alternatives are possible:
- The source and receiver are positioned at a distance of 60 m; at this distance the beam covers sufficiently all receiver pupils, which are provided with a calibrated diaphragm reducing the pupil diameter; also the source pupil is provided with a diaphragm in order to limit the signal level
- Next the irradiance level of the source at this range is determined at various locations of the beam and for various positions of the diaphragms over the source pupil, in order to test its homogeneity at both locations
- The responsivities of the receiver channels are separately measured with and without optics with the help of a 900K blackbody source and a standard tungsten strip lamp with a colour temperature of 2600K, both at short range (10 m)
- The transmission τ of the retro-reflector is measured for each channel at zero range with the help of the source and receiver, both provided with diaphragms in a complex set-up, with and without retro-reflector.

The retro-reflector excludes the use of short-range calibration, as the return beam, arriving back to the receiver, is too small. When the divergence of the return beam is enlarged in order to cover all receiver pupils, the mirror M should be displaced, when the system is going to be used at long range. Therefore we decided to carry out an outdoor system calibration with the retro-reflector located at a distance of 1668 m. In this way we also excluded the contribution of scattering (glare) effects in the optical system of the source and the retro-reflector. It appeared, that the alignment of the retro-reflector was not critical with respect to the direction and the divergence of the return beam. The alignment of the source could be done easily, because the signal level from the receiver could be monitored directly at the same location. However the positioning of the small mirror in the retro-reflector was very critical with respect to the signal level. At that time it was not possible to measure the irradiance distribution over the return beam in the area of the receiver pupils. The magnitude of the atmospheric scintillation effect appeared to be very large, reason why accurate signal reading in the time constant of the signal averaging circuit was not possible. The signal fluctuations due to scintillation exceeded by far the detector noise levels.

Moreover, when the position of the small mirror is set for a distance of 1668 m, which is 0.15 mm from the real focal plane of the main mirror, it has to be slightly repositioned for a measurement range of 890 m, which makes this pre-trial field calibration method unreliable. It has to be realised, that a change in small mirror position of 0.1 mm, gives already a change in signal level of about 30%. Thus when installing the transmissometer in a hot environment after calibration in a cool environment, it is highly recommended to apply an additional in-situ calibration. The linear expansion of the mirror system in the retro-reflector is more than 0.1 mm when the ambient temperature change is more than 20 °C. An in-situ calibration requires proper knowledge of the local weather conditions, at least at a certain number of periods. So during the UAE[2] campaign we looked for periods with the highest signal levels, which appeared regularly. The signal, collected by each of the receivers consisted of a block signal, one minute on and one minute off (Figure 7). The signals, returning from the retro-reflector and modulated with 800 Hz, were demodulated and averaged with a time constant of 1.1 sec. The shutter in the retro-reflector creates the block-signal shown, allowing further averaging over a two minute period, in order to improve the signal to noise ratio.
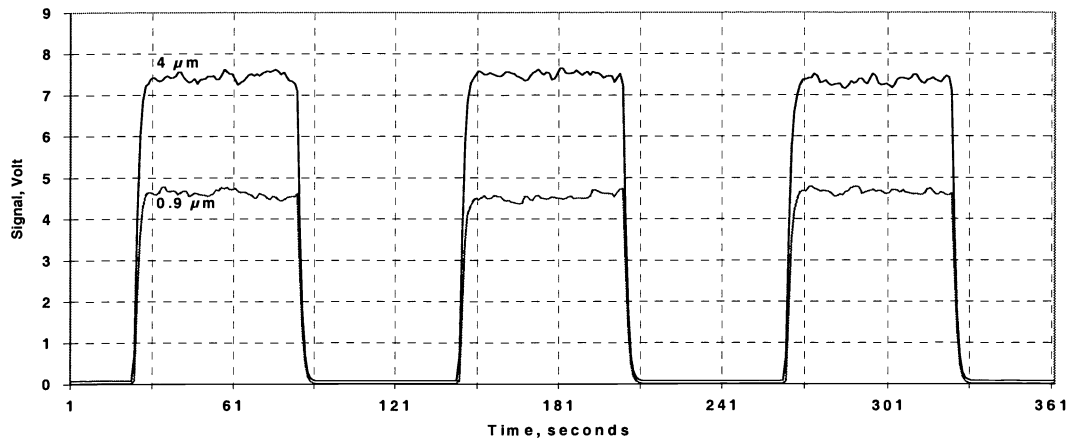

Figure 7. Examples of the raw signals of two of the MSRT channels during UAE[2]; 29 September 2004, 12.00 UTC

The signal graphs in Figure 7 show the returned signals, arriving via the retro-reflector. This was the case for the whole trial period, which implies that the backscatter by intervening atmospheric particles was negligible. Looking at the weather data, collected by our local weather station, it was found, that during several hours for most of the days (from 05.00-08.00 UTC = 09.00-12.00 local time), the air was warm and dry, so the absolute humidity was low (see Figure 8). In those periods, the visibility was generally good (about 10 km; the power station of Taweela was well visible). By applying the Modtran model, the atmospheric transmissions over a range of 2 x 890 m = 1780 m can be predicted for each of the MSRT spectral bands. The signal levels were subsequently coupled to these transmission values. Modtran was run for an air temperature of 37 °C, a relative humidity of 31% (absolute humidity = 13.6 g/m^3) and a rural aerosol model with a visibility of 10 km. The predicted molecular transmission varies from about 0.23 to 0.60 over the trials period for the 10 μm band.
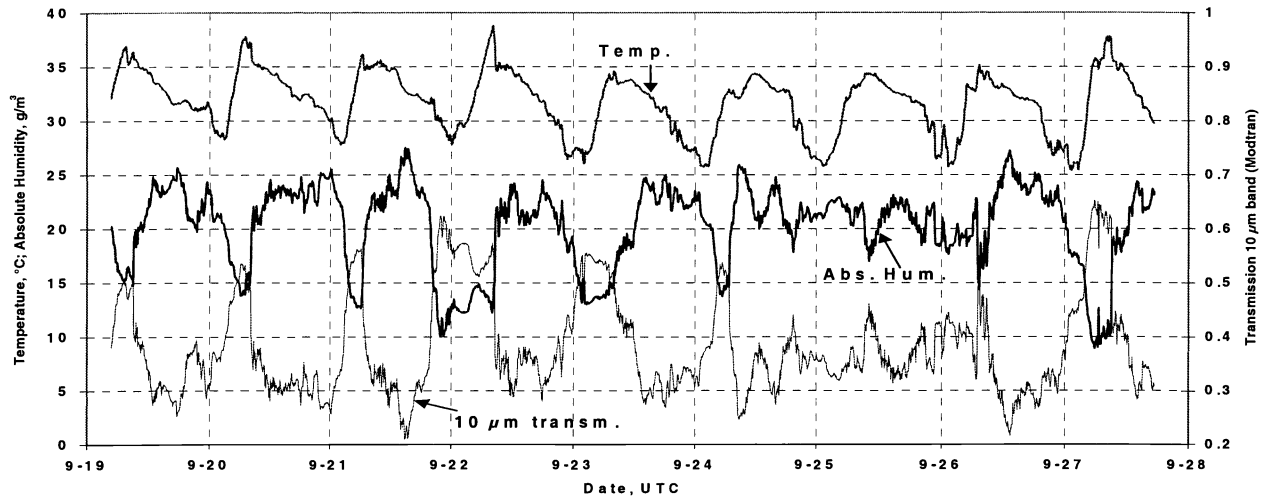
Figure 8. Weather data during the UAE[2] trials period, showing the air temperature, absolute humidity and atmospheric transmission by molecular effects according to Modtran

In table 2, a review is given of the predicted transmission in all the seven spectral bands, together with the measured signal levels at the given settings of the pre-amplifier gains. With the help of these data it is possible to convert directly the measured Voltages at any time into transmission levels.

Table 2. Review of in-situ MSRT calibration data during the UAE[2] experiments, based upon selected transmission data.

Channel	Band centre (μm)	Transmission from Modtran	Associated Voltage	Gain Setting
1	0.45	0.42	0.40	1000
2	0.6	0.54	1.05	10
3	0.9	0.60	4.5	10
4	1.5	0.52	6.0	10
5	2.3	0.67	9.0	1000
6	4	0.82	0.95	10
7	10	0.54	0.17	1000

5. IMPLICATIONS OF SCINTILLATION AND PATH-INHOMOGENEITY

In this section the consequences of atmospheric scintillation and possible inhomogeneities in atmospheric conditions along the path on measured signal values is considered in some detail. For this purpose we will compare two situations: one transmissometer set-up without and one transmissometer set-up with retro-reflector, while the total path length is the same in both cases: 2R. When the ray-tracing is compared for both cases for a refraction free atmosphere, it becomes clear that the extra intermediate optical element as formed by the retro-reflector, makes the probability of hitting the receiver optics considerably more critical. In Figure 9 both situations are schematically shown. In the set-up with the retro-reflector we simulate the optics by two lenses while the beam is focussed in the middle of them. For both lenses the obscuration by the 45° mirrors is shown in the centre of the lens.

The retro-reflector forms an obstruction in the central area of the path, through which, after adjustment of the small mirror M, a pencil beam of light b can pass to the receiver virtual image on the other side of the retro-reflector. As a consequence, one might expect that the system with retro-reflector will show more scintillation in a turbulent atmosphere than the one-way system because of the presence of two apertures, both leading to a certain intensity probability distribution in space and time [6]. In mono-static LIDAR systems with small retro-reflectors the returned rays follow nearly the same path in both directions, which may lead to enhanced backscatter (EBS) [7], resulting from the increased coherence at the receiver pupil due to nearly complete phase compensation for each point of each wave-front after double-passing the optical path. In our case however, to be considered as a bi-static set-up with incoherent source, the return beam is passing through an atmospheric path with a turbulence pattern, not correlated with that of the path of the outgoing beam, as their lateral distance is of the order of 10-40 cm (larger than for the case of small scale turbulence). Therefore phase differences in the wave-front, created on the way out, are not compensated at all on the way back to the receiver, where the beams tend to be largely incoherent, also due to the relatively short measurement path.
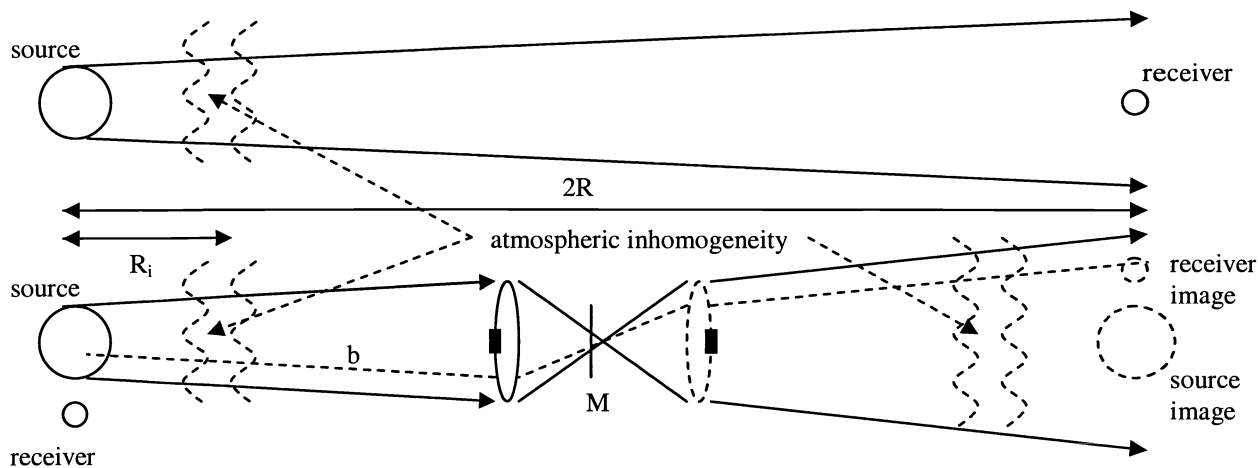

Figure 9. Ray paths for the one- and two-way transmissometer set-up, the lower one with simulated retro-reflector

For one-way systems, the ratio of the standard deviation (the root of the variance) of the signal and the mean signal is about proportional to the path-length [3, Chapter 2]. This predicted behaviour has been verified in various atmospheric propagation experiments [8, 9, 10]. It is not evident that this behaviour is the same for a two-way system. It may be expected that the (time averaged as well as turbulence-free) mean atmospheric transmission τ_1 for the one-way case with path-length 2R is the same as the square of the mean atmospheric transmission τ_2 of the signal for the two-way case with path-length R. The intensity fluctuations for the way out, described by the PDF_1 (Probability Density Function, assumed here to be lognormal: $\exp(-x^2/2\sigma_1^2)$ with $x=\ln(I_1/<I_m>)$ with variance σ_1^2 and a 4th moment $3\sigma_1^4$ (corresponding to the signal spikes) at the plane of the entrance pupil of the retro-reflector differ from the intensity fluctuations for the way back (another lognormal PDF_2 with random variable y: $\exp(-y^2/2\sigma_2^2)$, $y=\ln(I_2/<I_m>)$ with variance σ_2^2 and another 4th moment $3\sigma_2^4$, where $\sigma_2>\sigma_1$) due to the differences in aperture sizes. The combined PDF has a variance of $(\sigma_1^2+\sigma_2^2)$ and a 4th moment of $3(\sigma_1^2+\sigma_2^2)^2$, apparently greater than the 4th moment $3(4\sigma_1^4\tau_2^2)$ of a one-way system with the same total path-length. This expected effect corresponds to the experimental findings, showing rather spiky return signals.

In Figure 9 a location with a possible inhomogeneity in atmospheric conditions is shown, either in aerosol density or in strength of turbulence. It is clear that both set-ups react differently on this kind of conditions. The location of the area is critical with respect to the signal level and the blur at the location of the receiver. In the case of local turbulence in the one-way set-up, a location near the source provides small variations in angle of arrival for the rays, arriving at the receiver (small blur), while a location near the receiver provides large variation in angles of arrival (large blur) [11]. For the two-way set-up, the location of the turbulence area is of less importance due to the twice crossing of the area; a kind of averaging occurs. The turbulence effect is the smallest when the location of the turbulence area is near the retro-reflector. In the case of local aerosols, a similar conclusion may be drawn; the two-way set-up is somewhat favorable due to the averaging effect.

6. RESULTS

A selection has been made of samples of transmission data, in periods, where the weather changed significantly. In general the weather reproduced nicely each day, typically with lots of sunshine and wind-speeds, building up to 6 m/s in the afternoon, bringing a humid sea breeze from the northwest. Due to the (for transmission measurements) relatively short measurement path, no spectacular signal drops to the zero level were found and no heavy sandstorms did occur during our measurement period. Figures 10 and 11 show representative transmission data for four days: 20, 24, 25 and 28 September. On most of these days interesting changes in weather conditions did occur, especially concerning the absolute humidity during the change in wind direction in the morning around 7-8 o'clock UTC (=3-4 o'clock local time). The dry desert air is replaced by the humid air mass from the sea.
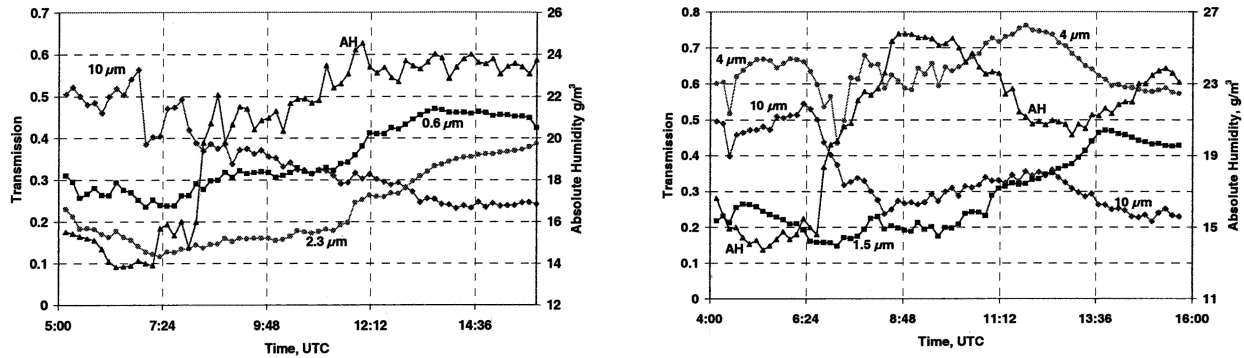
Figure 10. Transmission data for 20 September, 05.00-16.00 UTC (left) and 24 September, 04.00-1600 UTC (right)
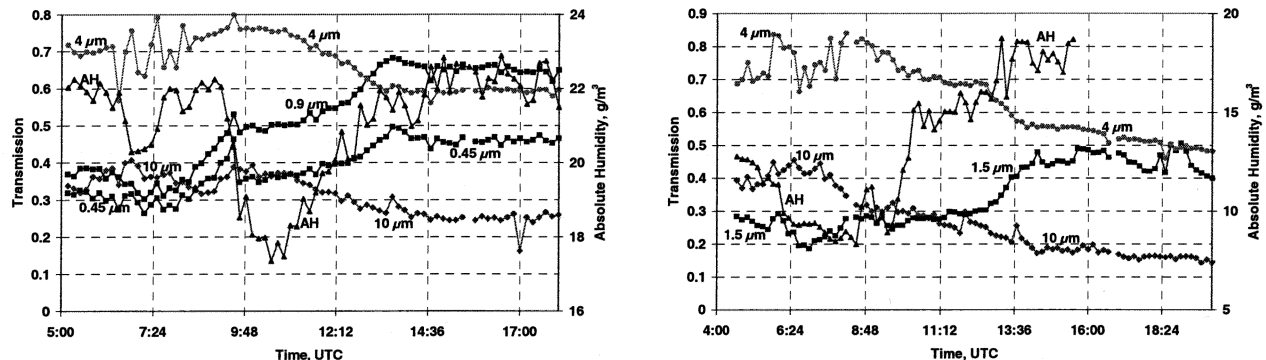

Figure 11. Transmission data for 25 September, 05.00-18.00 UTC (left) and 28 September, 04.40-20.20 UTC (right)

The signals in the channels 1-5 (0.4-2.5 μm) show a normal behaviour in changing visibility conditions during the day. The signals in the 4 μm and 10 μm bands however, depend strongly on the absolute humidity. For the 10 μm band, this is a well known phenomenon, but for the 3.6-4.1 μm band water vapour should have only a minor effect on the extinction coefficient. In order to separate the aerosol contribution from the total transmission, the molecular extinction has been calculated for the 4 μm and 10 μm bands of the MSRT. Next the total transmission is divided by this value to obtain the aerosol transmission: 4 μm(aer) and 10 μm(aer). We consider this ratio to be just caused by the extinction from aerosols. Figure 12 shows the result of this procedure for two representative days: 23 and 26 September. It is interesting to see, that for the 10 μm band, the aerosol contribution is relatively small, while in the 4 μm band aerosols apparently play an important role in humid conditions. It is noted, that some of the fluctuations in the 10 μm(aer) transmission rise above the value of 1, probably due to refraction (low-frequency scintillation), forward scattering effects or spurious retro-reflectors. Unfortunately the measurements did not run 24h/24h, so we miss data for most of the nighttime periods.
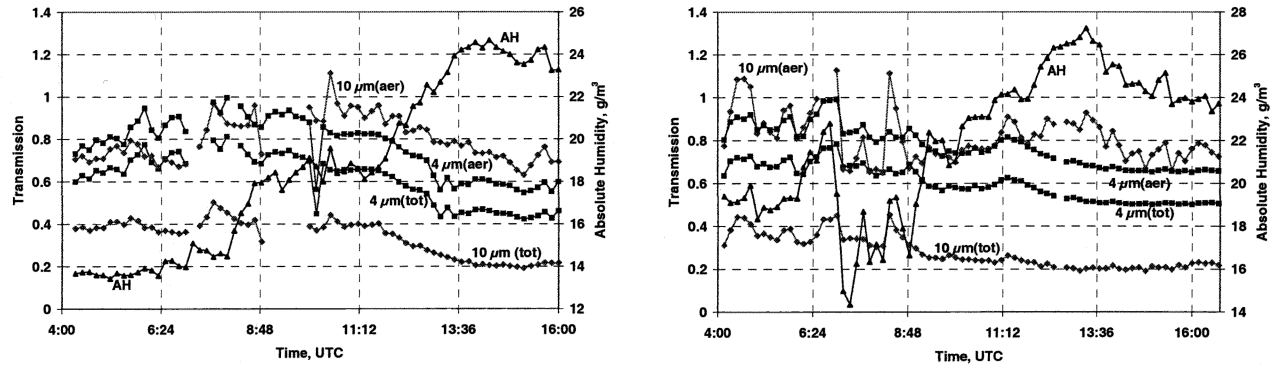
Figure 12. Transmission data for 23 September, 04.20-16.00 UTC (left) and 26 September, 04.10-16.40 UTC (right); the plots show measured data and transmission plots, from which the molecular extinction is removed

7. DATA ANALYSIS

The transmission data can further be analysed by plotting the transmission in one spectral band against the transmission in another spectral band. The slopes of the plots are determined by the extinction coefficients in the various bands, which on their turn are determined by the particle characteristics. Selections of these plots are presented in Figures 13 and 14. In these plots the 10 μm(aer) transmission data have been used. For the other bands the total transmission values were taken, as the spectral absolute humidity effect is small in those bands. The plots show again that the 4 μm transmission decreases with increasing humidity, while the transmission in the bands 1-5 increases. This is probably due to the bigger particles arriving from the sea with sizes of the order of 3 μm, with considerably less extinction in the 10 μm band. This should be checked with data from the NRL particle samplers. The number of smaller particles (<0.3 μm), determining the extinction in the shorter spectral bands, decreases at the same time. The creation of larger particles during the morning can also be observed from the AERONET data [see AERONET site], in which also particles with a size of about 3 μm are predicted as a result of the retrieval from the data of the local multi-spectral sun-photometer system.
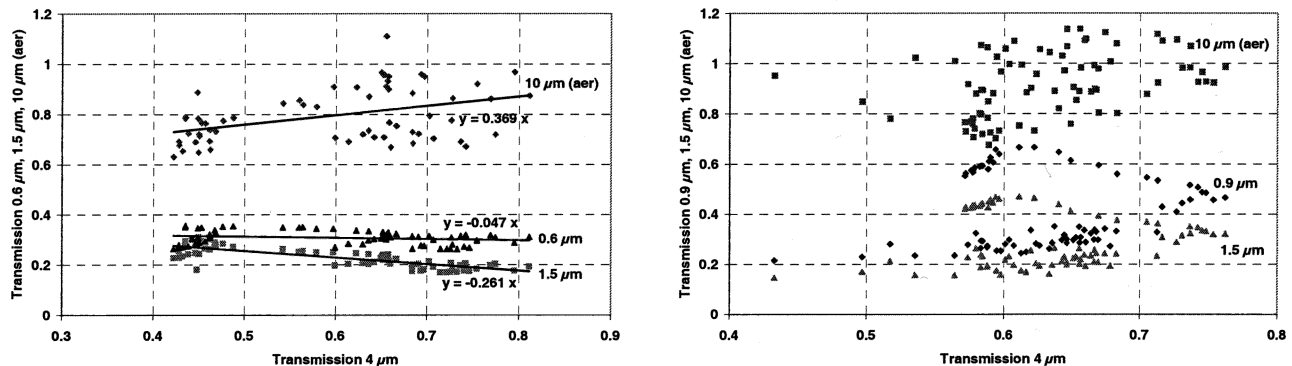

Figure 13. $\tau_a(\lambda_1)$- $\tau_a(\lambda_2)$ plots for 23 September 04.20-16.00 UTC (left) and 24 September 04.00-16.00 UTC (right)

In periods, including the rise and fall of the absolute humidity, the plots show a different behaviour for both conditions (24 and 28 September). In Figure 13 (right), the lower part of the 0.9 μm transmission data correspond to the early part of the morning, while the upper part corresponds to the later part of the day. The lower parts of the 0.9 μm and 1.5 μm plots have a very small positive slope in the morning, while the slope is negative for the later part of the day. In Figure 14 (right) the left part of the 0.45 μm data correspond to the night data of the 28th of September, showing a positive slope with the 4 μm transmission data, while the slope is negative most of the time.
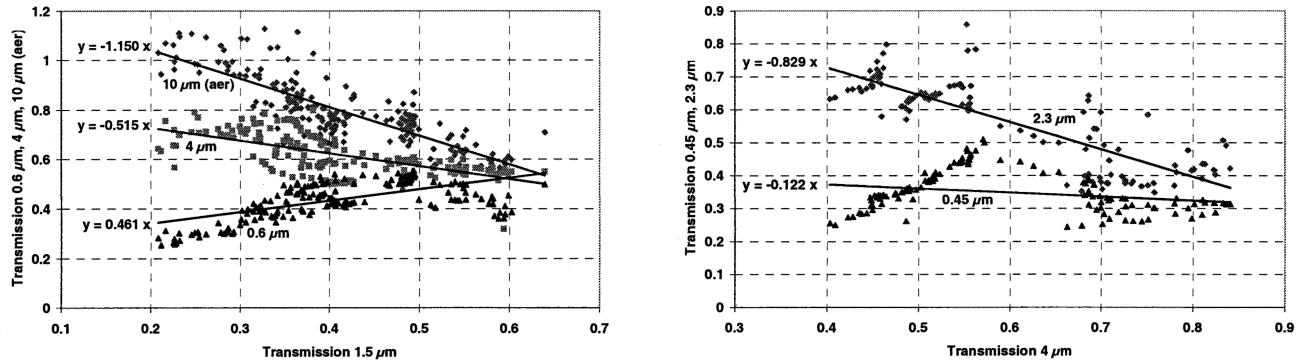
Figure 14. $\tau_a(\lambda_1)$- $\tau_a(\lambda_2)$ plots for 25/09, 05.10 - 26/09, 16.40 UTC (left) and 28/09, 04.40 - 29/09, 01.20 UTC (right)

This is also the case with most of the comparisons of the transmission data in the 10 μm band with the data in the short wave bands. It can be concluded that the infrared transmission in the 4 μm band, normally favorable in tropical areas, is much less than expected according to standard propagation models such as Modtran. The transmission in the 10 μm band does not strongly deviate form the model predictions; the particle size is apparently too small for that. It is recommended to continue the data analysis, when more physical data on the particles are available.

ACKNOWLEDGEMENTS

REFERENCES

[1] W. Michael Farmer, *The Atmospheric Filter*, Volume 1, Sources; JCD Publishing, Winter Park, FL; 2001

[2] Arie N. de Jong et al, *Multi-band optical/IR transmissometry during the VAMPIRA trials, spring 2004*, SPIE Volume 5572, Optics in Atmospheric Propagation and Adaptive Systems VII, Gran Canaria, September 2004

[3] The Infrared &Electro-Optical Systems Handbook, Vol. 2 Atmospheric Propagation of Radiation, Chapter 1.4, *Atmospheric Scattering*, SPIE Opt. Eng. Press, 1993

[4] Arie N. de Jong et al, *Long-range transmission at low elevations over the ocean*, Proc. Symposium RTO-MP1 on "E-O propagation, signature and system performance under adverse meteorological conditions", Naples, March 1998

[5] Carl R. Zeisse et al, *Measurement of low-altitude infrared propagation*, Applied Optics, Vol.39, No. 6, pp 873-886, Febr. 2000

[6] Arie N. de Jong, *Intensity variations of small incoming airborne targets, popping-up above the horizon*, SPIE Volume 5237, Optics in Atmospheric Propagation and Adaptive Systems VI, Barcelona, September 2003

[7] Larry C. Andrews et al, *Laser Beam Scintillation with Application*, SPIE Press, Bellingham, WA, 2001

[8] Arie N. de Jong et al, *Point target extinction and scintillation as function of range at LAPTEX, Crete*, SPIE Volume 3125, Propagation and Imaging through the atmosphere, San Diego, July 1997

[9] Arie N. de Jong et al, *Scintillation measurements during the EOPACE November '96 and August '97 campaigns*, SPIE Volume 3433, Propagation and Imaging through the atmosphere, San Diego, July 1998

[10] Arie N. de Jong et al, *TG16 point target detection experiment POLLEX, Livorno 2001*, SPIE Volume 4820, Infrared Technology and Applications XXVIII, Seattle, July 2002

[11] Arie N. de Jong, *Geometrical image distortion and aberration for long-range targets in a non-homogeneous atmosphere*, SPIE Volume 5572, Gran Canaria, September 2004